Proton resonances in ^{32}S from $E_x = 9.83$ to 12.74 MeV

D. F. Fang, E. G. Bilpuch, and C. R. Westerfeldt
Duke University, Durham, North Carolina 27706
and Triangle Universities Nuclear Laboratory, Duke Station, Durham, North Carolina 27706

G. E. Mitchell
North Carolina State University, Raleigh, North Carolina 27695
and Triangle Universities Nuclear Laboratory, Duke Station, Durham, North Carolina 27706
(Received 31 August 1987)

Differential cross sections for the ^{31}P(p,p$_0$), (p,p$_1$), (p,α_0), and (p,α_1) reactions were measured in the range $E_p = 1.00$ to 4.01 MeV with an overall resolution of about 400 eV. The resonance parameters were extracted for 143 levels with a multilevel, multichannel R-matrix code. These parameters include resonance energy, total angular momentum, parity, partial widths, channel spin or orbital angular momentum mixing ratios, and, for some resonances, the relative signs of width amplitudes. Eight isobaric analog resonances were identified in ^{32}S. Proton resonance strengths were compared with shell model predictions. The ^{31}P(p,α_0) data were used to obtain the reaction rates for the inverse reaction ^{28}Si(α,p$_0$).

I. INTRODUCTION

The structure of ^{32}S below $E_x = 11$ MeV has been well studied, although there have been few measurements since the compilation by Endt and Van der Leun[1] in 1978. An extensive study of ^{32}S was performed by Kalifa *et al.*[2] with the ^{31}P(^{3}He,d)^{32}S reaction. In the region from $E_x = 11$ MeV to the ^{16}O+^{16}O threshold at 16.54 MeV, there is little information. Above this threshold many experiments have been performed with heavy ions.

In the present experiment, ^{32}S was studied by proton scattering from ^{31}P. This measurement is part of a program investigating odd-mass target nuclei in the 2s-1d shell. Previous targets studied include ^{29}Si (ground state $J^\pi = \frac{1}{2}^+$), ^{27}Al ($\frac{5}{2}^+$), ^{25}Mg ($\frac{5}{2}^+$), and ^{23}Na ($\frac{3}{2}^+$).[3-7] Although the resonance analysis is much more complicated than for zero spin targets, a wealth of spectroscopic information is obtained. These results are important for such topics as stretched states, astrophysical reaction rates, analog states, and spin-spin interactions, as well as for comparison with nuclear structure calculations.

The present high resolution measurement fills an important gap in the existing data on ^{32}S. There is a shell model calculation[2] for the positive parity levels in ^{32}S up to $E_x = 14.60$ MeV. In the lower energy region ($E_x \leq 11$ MeV), the shell model works very well. However, there were no data at higher energies to compare with these calculations. The ^{31}P(p,α_0) channel is open throughout the entire energy range of the present experiment. Resonances with strong alpha decay in ^{32}S are interesting, since information about resonances with large alpha parentage provides a test for cluster models. For astrophysics, the resonance parameters for the ^{31}P(p,α_0) reaction can be used to evaluate thermonuclear reaction rates for the inverse reaction by use of the principle of detailed balance.

The high resolution system, experimental equipment, and the data acquisition procedures are described in Sec. II. Analysis of resonances in the ^{31}P(p,x) reactions and a discussion of level-level interference effects are given in Sec. III. The new spectroscopic information for ^{32}S in the excitation energy range $E_x = 9.83$–12.74 MeV is presented and discussed in Sec. IV, and a summary is given in Sec. V.

II. EXPERIMENTAL PROCEDURE

This experiment was performed with the KN Van de Graaff accelerator and associated high resolution system at TUNL. A detailed description of the system, including recent improvements and modifications, is given by Westerfeldt *et al.*[8] The system provides an overall energy resolution of 300–400 eV for thin solid targets in the range of proton beam energy $E_p \sim 1$–4 MeV. Proton-induced reactions were measured from $E_p = 1.00$–4.01 MeV at laboratory angles 90°, 127°, 145°, and 165° with surface barrier detectors. In order to measure the ^{31}P(p,α_1) reaction above $E_p = 2.98$ MeV, transmission detectors were employed at 108°, 135°, and 165° to detect α_1 particles; particle identification was required because the α_1 particles generate the same pulse height in the surface barrier detectors as protons elastically scattered from ^{16}O. In practice the (p,p$_1$) reactions were observed above $E_p = 2.18$ MeV and the (p,α_1) reaction above $E_p = 2.98$ MeV. The solid angles for the detectors were adjusted such that the counting rate for Rutherford scattering at each detector is approximately equal.

Targets were prepared by evaporating Zn_3P_2 onto ultrapure Ni coated (~ 0.5 μg/cm^2) carbon foils (4–5 μg/cm^2). The targets contained 1–3 μg/cm^2 of ^{31}P. Ni was added to the backing because it enhances both target stability and uniformity. Targets prepared in this

manner proved stable at 2–3 μA beam current.

The data acquisition was supported by a VAX 11/750 computer and a general data processing software XSYStem.[9] The yield curves for the ^{31}P(p,p$_0$), (p,α_0), (p,p$_1$), and (p,α_1) reactions were obtained from the spectra, which were monitored online and stored for more detailed offline analysis. Data were measured in energy steps of 100–400 eV, depending on the resonance structure. The counting statistics were better than 2%. Most of the data in the present experiment were measured twice to ensure reproducibility. Absolute energy calibration for the system was performed with secondary standards [^{44}Ca(p,p) and ^{56}Fe(p,p) reactions], which were calibrated with respect to primary neutron threshold standards: ^{7}Li(p,n) at E_p=1.8804 MeV and ^{13}C(p,n) at E_p=3.2357 MeV. The uncertainty for absolute resonance energies is about 3 keV.

III. RESONANCE ANALYSIS

Experimental excitation functions for the four particle channels were fitted with the multilevel, multichannel R-matrix program MULTI6, which is based on the differential cross section expression of R-matrix theory given by Lane and Thomas.[10] The code MULTI6 generates the theoretical excitation functions with a given set of resonance parameters: resonance energies, J^π values, and laboratory partial widths. The calculated excitation functions are then compared with the experimental data. The fitting is performed by trial and error, with all resonance parameters adjusted to achieve the best visual fit. A general description of the analysis procedure for nonzero spin targets was given by Nelson *et al.*[11]

For a target of spin I and a projectile of spin i, the two spins are coupled to form a channel spin s, and the channel spin is then combined with the relative orbital angular momentum l to form the spin J of the compound nuclear state. For a given J^π value and a nonzero spin target, there are usually several channels with various l,s combinations which can form the state. Coupling a proton (spin $\frac{1}{2}$) and a ^{31}P target (ground state spin $\frac{1}{2}$) gives channel spin values 0 and 1. The combination of channels with the same l value and different s values is called channel spin mixing (s mixing), while the combination of channels with the same s and different l values is called angular momentum mixing (l mixing). For an unpolarized beam on an unpolarized target, the two channel spin contributions add incoherently. The angular distributions of the reaction products are functions of the s-mixing and l-mixing ratios. The channel spin mixing ratio for elastic scattering is

$$\xi=\sum_l \Gamma_{p,s=1,l}/(\Gamma_{p,s=1,l}+\Gamma_{p,s=0,l}) ,$$

where $\Gamma_{p,s,l}$ is the proton laboratory width with orbital angular momentum l and channel spin s. The l-mixing ratio is

$$\varepsilon=\tan\Psi=\pm(\Gamma_{p,s,l+2}/\Gamma_{p,s,l})^{1/2} .$$

In practice, l mixing is usually small unless the compound nucleus has a configuration[2] which strongly prefers $l+2$ partial waves. Since the laboratory width is proportional to the penetrability P_l, which decreases rapidly with l, only partial waves with $l<4$ need be considered.

The analysis is simpler when the resonance widths are larger than the energy resolution Δ. For a resonance width Γ less than Δ, both J and the s-mixing ratio usually cannot be uniquely determined. Such ambiguities also occur for resonances with higher J values and small laboratory widths. Thus good experimental resolution is very important, not only for separation of overlapping resonances, but also for determination of the resonance parameters.

Interference between levels has dramatic effects on the resonance shapes. Consider the two level, many channel case. There are two kinds of interference, involving levels with different J^π and levels with the same J^π. Although the R matrix is block diagonal in J, the expression for the differential cross section is summed over all J. Thus for overlapping resonances with different J values, there is a two level interference term. With resonance parameters $J_1^{\pi 1}$, $J_2^{\pi 2}$, l_1, l_1', l_2, and l_2', the interference term in the cross section can be written as

$$\left[\frac{d\sigma_{\eta,\eta'}}{d\Omega_{\eta'}}\right]=\frac{1}{2k_a'^2(2s+1)}\sum_{ss'l_1l_1'}\frac{(-1)^{s-s'}\Gamma_{1c}^{1/2}\Gamma_{1c'}^{1/2}\Gamma_{2c}^{1/2}\Gamma_{2c'}^{1/2}\cos(\delta+\delta_2-\delta_1)}{[(E_1-E)^2+\frac{1}{4}\Gamma_1^2]^{1/2}[(E_2-E)^2+\frac{1}{4}\Gamma_2^2]^{1/2}}\bar{Z}(l_1J_1l_2J_2,sL)\bar{Z}(l_1'J_1l_2'J_2,s'L)P_L(\cos\theta_{\eta'}) ,$$

where $\delta=\omega_{l_1}+\omega_{l_1'}-\omega_{l_2}-\omega_{l_2'}+\phi_{l_2}+\phi_{l_2'}-\phi_{l_1}-\phi_{l_1'}$, with ω the Coulomb phase shift and ϕ the hard sphere phase shift, $\delta_\lambda=\tan^{-1}[\Gamma_\lambda/2(E_\lambda-E)]$ is the nuclear resonance phase shift, and $c=\{\alpha sl\}$ is the channel label. From the symmetry properties of the Z coefficients, the selection rules for the interference term are l_1+l_2-L=even and/or $l_1'+l_2'-L$=even. For states with opposite parities the interference term contains only Legendre polynomials with odd L values, while for states with the same parity (but different J) only Legendre polynomials with even L values occur. The interference effects are dominated by the largest terms in the product of partial width amplitudes $\Gamma_{1c}^{1/2}\Gamma_{1c'}^{1/2}\Gamma_{2c}^{1/2}\Gamma_{2c'}^{1/2}$ with specific $\{s,s',l_1,l_1',l_2,l_2'\}$ values. The overall sign of the product is important: the interference effects can be maximized or minimized by changing relative signs of these partial width amplitudes. (A different level-level interference effect arises for two levels with the same J^π. An example in Ref. 11 illustrates that relative signs can have large effects for that case.)

In the present experiment we observed interference effects which were sensitive to the relative signs for reso-

TABLE I. Level interference effects in ^{31}P(p,α_0).

Resonance 1 ($J^\pi=1^-$)				Resonance 2 ($J^\pi=2^+$)				$(-)^{s-s'}\Pi^a$	
s	Γ_p[b]	s'	Γ_α	s	Γ_p	s'	Γ_α	(keV)^2	Figure
0	8.50	0	3.00	0	0.15	0	0.14	0.73	1(a)
1	−10.50[c]			1	0.03			0.36	
0	−8.50[c]	0	3.00	0	0.15	0	0.14	−0.73	1(b)
1	10.50			1	0.03			−0.36	
0	8.50	0	3.00	0	0.15	0	0.14	0.73	1(c)
1	10.50			1	0.03			−0.36	
0	8.50	0	−3.00[c]	0	0.15	0	0.14	−0.73	1(d)
1	10.50			1	0.03			0.36	

[a]$\Pi=\Gamma_{1c}^{1/2}\Gamma_{1c'}^{1/2}\Gamma_{2c}^{1/2}\Gamma_{2c'}^{1/2}$.
[b]Resonance widths are in keV. For resonance 1, $l=l'=1$ and for resonance 2, $l=l'=2$.
[c]Signs are associated with the resonance width amplitude $\Gamma_c^{1/2}$.

nances with the same J^π and with different J^π. As an illustration, we present results for two levels with different J^π. Table I lists the partial widths and the product term of the partial width amplitudes for two states in ^{32}S. Resonance 1 is a broad 1^- state at $E_p=2.0220$ MeV, which has a large α_0 width, while resonance 2 is a narrow 2^+ state at $E_p=2.0233$ MeV. In the α_0 decay channel there is only one value of s' and l' for each resonance. Thus only two terms in the partial width amplitude products are left in the summation for the (p,α_0) reaction with target spin $I=\frac{1}{2}$. The two terms can be both positive, both negative, or have opposite signs [together with the phase factor $(-1)^{s-s'}$]; these four combinations are listed in the next to last column in Table I. Figure 1 illustrates these effects at 127° and 165° for the four sign combinations. Only one combination [panel (a)] fits the data well at these (and other) angles. The interference shape will be the same if the sign of the resonance partial width amplitude is assigned to either resonance. In Table I, the signs are associated with resonance 1.

IV. RESULTS

A. General

In the present experiment excitation functions were measured in the range $E_p=1.00$–4.01 MeV, and a total of 143 resonances were observed. Resonances above $E_p=2.05$ MeV had not been analyzed previously except for a 4^-, $T=1$ state and a 0^+, $T=2$ state near $E_p=3.285$ MeV. The excitation functions for (p,p$_0$) and (p,α_0) in the energy range 1.00–2.00 MeV are shown in Fig. 2; the excitation functions for (p,p$_0$), (p,α_0), and (p,p$_1$) in the range $E_p=2.00$–3.00 MeV are shown in Fig. 3; the excitation functions for ^{31}P (p,p$_0$), (p,α_0), (p,p$_1$), and (p,α_1) in the range $E_p=3.00$–4.00 MeV are shown in Fig. 4. Typical uncertainties in the resonance parameters are about 10% for small resonances. For large resonances ($\Gamma\geq 15$ keV) the laboratory widths have larger uncertainties ($\sim$20%), especially for resonances whose inelastic widths are larger than their elastic widths.

There is good agreement with the previous data compiled by Endt and Van der Leun[1] below $E_p=2.050$ MeV. Due to small elastic widths, several resonances observed below $E_p=2.00$ MeV in the (p,γ) experiments are barely seen in the present measurement. For these resonances the laboratory widths have large uncertainties; their J^π values are taken from Endt's compilation. The major disagreements are the following: (1) the resonance at $E_p=1.643$ MeV whose J^π value was assigned previously as 1^-, is assigned $J^\pi=0^+$ from the present data. (2) The resonance $E_p=1.796$ MeV was assigned previously as $J^\pi=2^+$, with α_0 decay. In the present experiment the resonance shape in elastic scattering is quite different from that for a 2^+ resonance, and no α_0 decay was observed. This resonance is assigned $J^\pi=1^-$. (3) The resonances at $E_p=1.280$, 1.724, and 1.740 MeV, which were observed in the (p,γ) reaction, are not seen in the present experiment.

Five new resonances were observed in the region $E_p=1.900$–2.050 MeV. The J^π value for the resonance at $E_p=1.989$ MeV was uncertain in the previous data; the present experiment provides evidence for a 1^- assignment. There are no resonance parameters available for comparison above $E_p=2.050$ MeV. To avoid introducing spurious resonances, a level is assigned only if there is clear evidence for its existence. Because of space limitations, the extracted resonance parameters and the relative signs of the resonance amplitudes are not tabulated here. A complete listing is available from the authors.

B. Analog states

Analog state identification requires information about the parent state. Such information can be obtained by neutron transfer experiments, usually (d,p) reactions. The strengths of the corresponding states in parent and daughter nuclei are assumed to be equal:

$$s_{dp}=s_n\approx s_p=(2T+1)\frac{\Gamma_p}{\Gamma_{s.p.}},$$

where s_p is the proton analog spectroscopic factor, which characterizes the strength of the analog state, Γ_p is the measured laboratory width of the analog state,

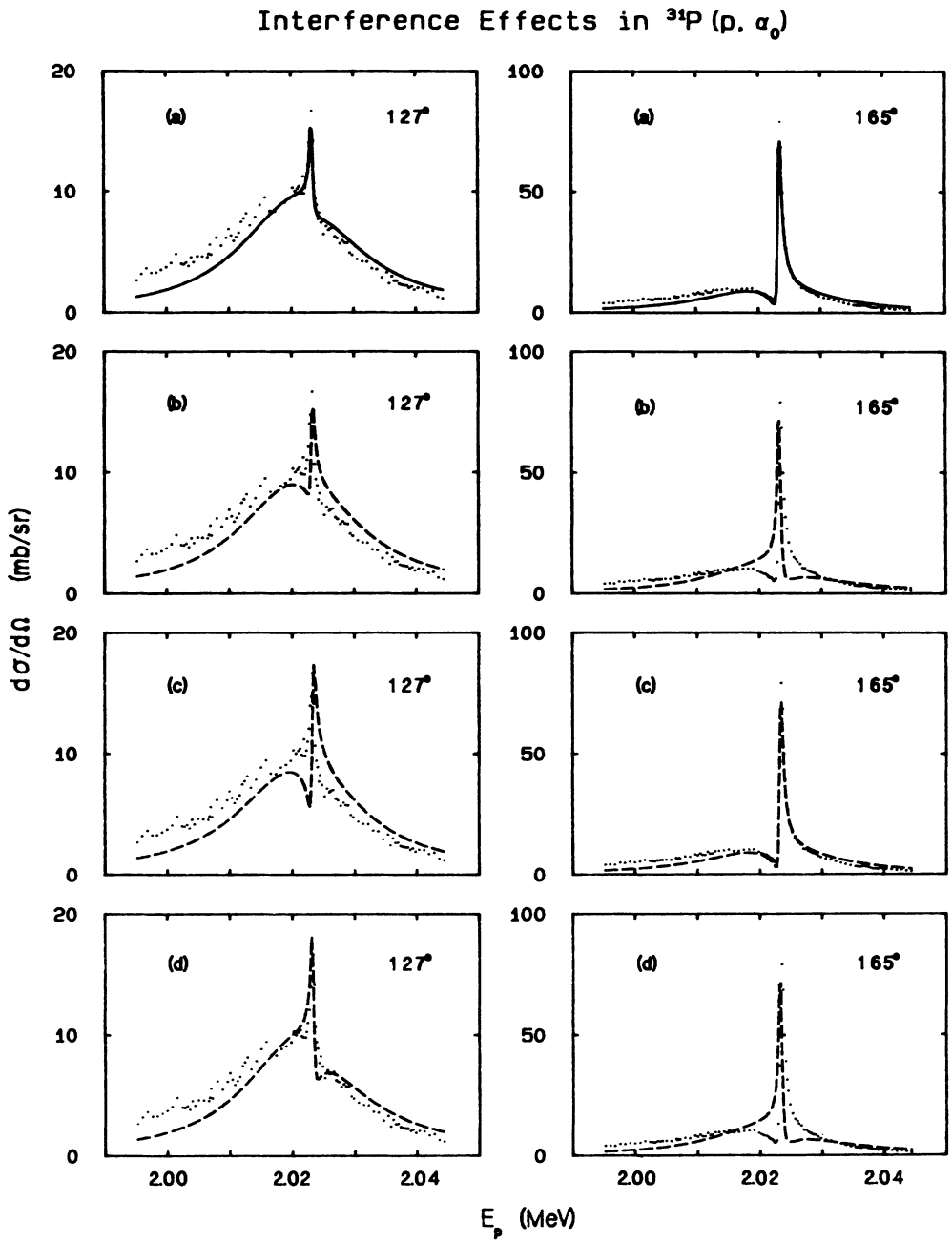

FIG. 1. Two level interference effects in the ^{31}P(p,α_0) reaction at 127° and 165°. There is a broad 1^- resonance with a narrow 2^+ resonance superimposed. The dots are the experimental data and the solid curve in (a) is the fit with the $s=0$ proton partial width amplitude positive, the $s=1$ proton amplitude negative, and the alpha amplitude positive. Only relative signs between the two resonances matter; the signs are arbitrarily assigned to the 1^- resonance. Resonance parameters are listed in Table I. The dashed lines in (b), (c), and (d) represent the calculated cross section with the same resonance parameters except for signs of the partial width amplitudes. The sign combination used in part (a) is the only solution which fits the data at both angles.

$s_{dp} \equiv s_n$ is the neutron spectroscopic factor, $\Gamma_{s.p.}$ is the single particle width of the proton resonance, and T is the isospin of the states.

The identification of analog states and the calculation of analog spectroscopic factors is described by Bilpuch *et al.*[12] The proton single particle widths for the analog resonances were calculated with the ZDH (Refs. 13 and 14) method. To facilitate comparison with (d,p) data, the potential well parameters are those used in the (d,p) analysis.

Previous experiments[1] identified the $T=1$ analog resonances below $E_x(^{32}\text{S})=10.977$ MeV; these correspond to

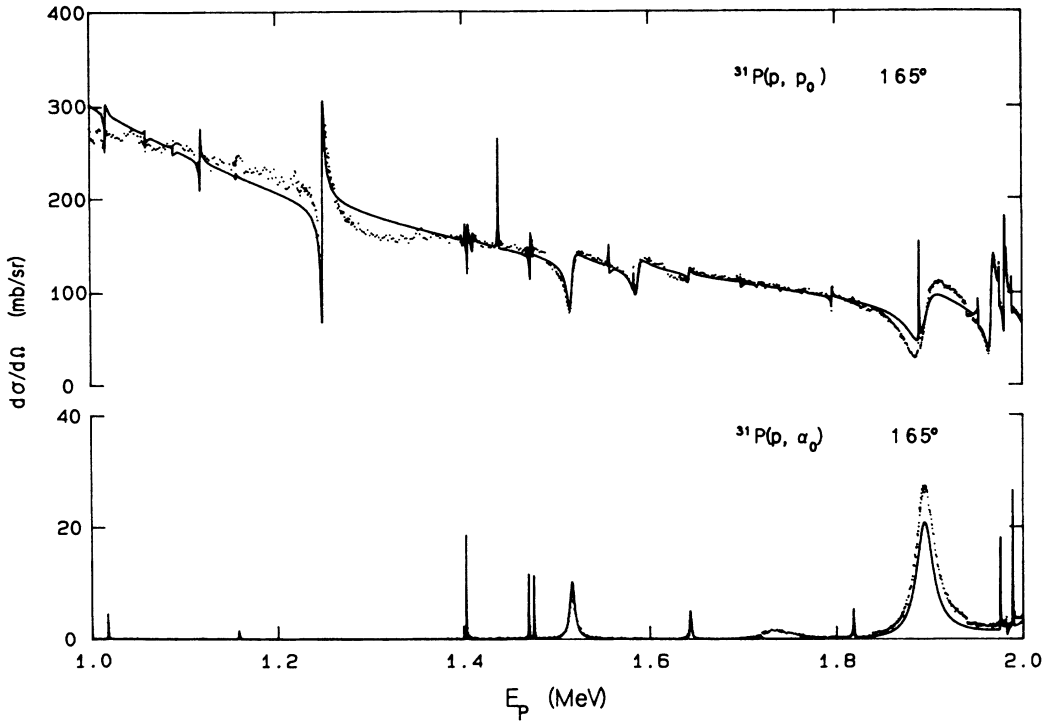

FIG. 2. Differential cross sections for $^{31}P(p,p_0)$ and $^{31}P(p,\alpha_0)$ at 165° in the energy range $E_p = 1.00-2.00$ MeV. The solid curve is the R-matrix fit.

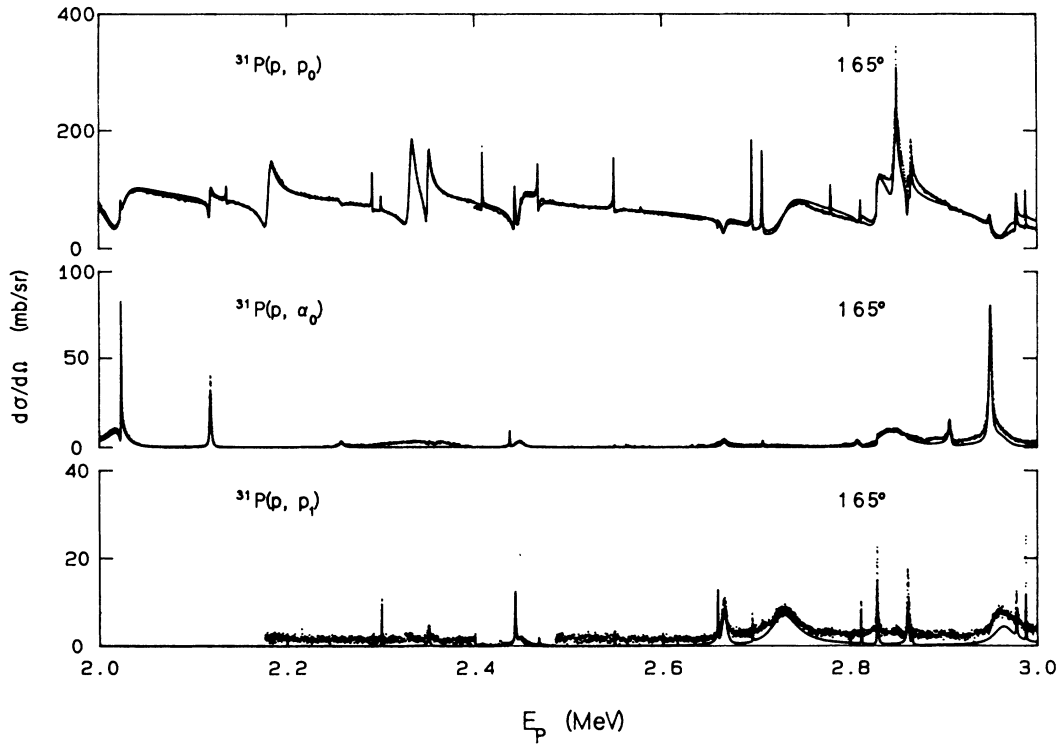

FIG. 3. Differential cross sections for $^{31}P(p,p_0)$, $^{31}P(p,\alpha_0)$, and $^{31}P(p,p_1)$ at 165° in the energy range $E_p = 2.00-3.00$ MeV. The solid curve is the R-matrix fit.

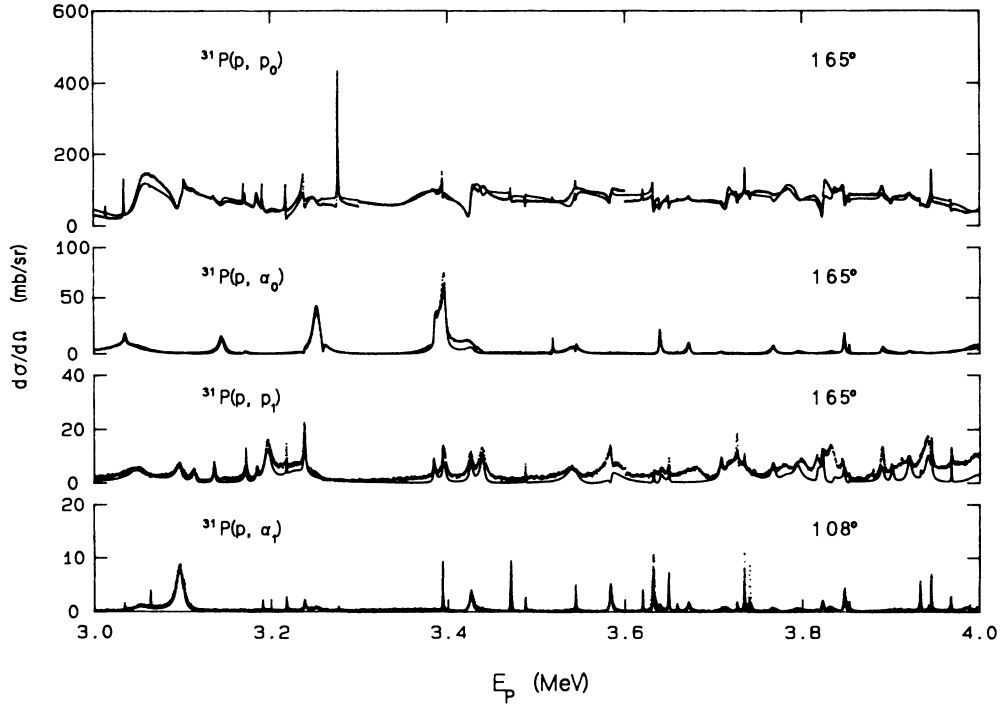

FIG. 4. Differential cross sections for ^{31}P(p,p$_0$), ^{31}P(p,α_0), and ^{31}P(p,p$_1$) at 165° and ^{31}P(p,α_1) at 108° in the energy range $E_p = 3.00$–4.00 MeV. The solid curve is the R-matrix fit.

proton bombarding energies up to 2.181 MeV. In addition, a 4^- analog resonance was identified at $E_x = 12.044$ MeV ($E_p = 3.282$ MeV). For the excitation energies of parent and daughter states of the well-studied $T=1$ analog resonances in ^{32}S below the proton separation energy, the average difference in excitation energy $E_x(^{32}\text{S}) - E_x(^{32}\text{P})$ is about 7.00 MeV. For resonances above $E_x(^{32}\text{S}) = 11.09$ MeV, only a few resonances are identified as analog states, mainly because of the lack of (d,p) data corresponding to this energy region.

The results for the analog states observed in the present experiment are listed in Table II. The agreement between the analog and parent state spectroscopic factors is excellent.

(1) The analog of the $E_x(^{32}\text{P}) = 3.320$ MeV, 3^- state is a resonance at $E_x(^{32}\text{S}) = 10.223$ MeV. Previous measurements suggest that this resonance may be mixed with a 3^-, $T=0$ resonance at $E_x(^{32}\text{S}) = 10.286$ MeV.

TABLE II. $T=1$ analog resonances.

^{32}P			^{32}S						
J^π	E_x (MeV)	s_n ($=s_{dp}$)[a]	J^π	E_x (MeV)	E_p (MeV)	Γ_p (keV)	$\Gamma_{s.p.}/(2T+1)$ (keV)	s_p	$E_x(^{32}\text{S}) - E_x(^{32}\text{P})$ (MeV)
2^-	3.260	0.44	2^-	10.075	1.250	1.50	3.53	0.42	6.815
3^-	3.320	0.44	3^-	10.223	1.403	0.016	0.037	0.43	6.913
4^-	3.443	0.78	4^-	10.257	1.438	0.035	0.048	0.73	6.814
			4^-	10.398	1.583	0.012	0.087	0.14	6.955
2^+	3.444	b	2^+	10.368	1.557	0.025	1.25	0.02	6.924
2^+	3.880	0.056	2^+	10.791	1.989	0.08	5.18	0.015	6.911
			2^+	10.824	2.023	0.17	5.57	0.030	6.943
2^-	4.010	0.066 ($l=1$)	2^-	10.977	2.181	6.60	55.00	0.13	6.967
		0.124 ($l=3$)				0.10	0.64	0.16	
1^-	4.040	0.43	1^-	10.823	2.022	19.0	42.00	0.45	6.782
3^-	4.150	0.026	3^-	11.092	2.300	0.03	1.03	0.029	6.942

[a]Endt and Van der Leun (Ref. 1).
[b]Masked by the resonance at $E_x(^{32}\text{P}) = 3.443$ MeV, see Ref. 2.

(2) The analog of the $E_x(^{32}\mathrm{P})=3.880$ MeV, 2^+ state was observed previously as a doublet in proton scattering. We observed two 2^+ resonances about 30 keV apart. The summed strength s_p agrees with the neutron strength s_n.

(3) The analog of the $E_x(^{32}\mathrm{P})=4.150$ MeV, 3^- state is a narrow resonance which was not observed previously.

(4) Above $E_x(^{32}\mathrm{P})=4.20$ MeV (corresponding to $E_p=2.41$ MeV), there are no suitable (d,p) data for comparison.

The fluctuations in the energy difference $E_x(^{32}\mathrm{S})-E_x(^{32}\mathrm{P})$ listed in Table II can be qualitatively explained in terms of the Thomas-Erhman shift.[10,15] For a state in the parent nucleus, the relation between the observed energy E_{rN} and the energy eigenvalue $E_{\lambda N}$ is

$$E_{rN}=E_{\lambda N}-\Delta_{\lambda N} ,$$

where $\Delta_{\lambda N}=\gamma^2_{\lambda N}[S_N(E_{rN})-B]$ is the energy shift, $\gamma^2_{\lambda N}$ is the neutron reduced width, and B is the boundary condition. There is a similar relation for the state in the daughter nucleus. Assuming that the reduced width γ^2_λ and the boundary condition B of the states in the two nuclei are equal, and subtracting the expression for E_{rN} from that for E_{rP}, yields

$$E_{rP}-E_{rN}=(E_{\lambda P}-E_{\lambda N})+[S_N(E_{rN})-S_P(E_{rP})]\gamma^2_\lambda .$$

The second term on the right-hand side is the boundary condition level displacement (Δ_{PN}) between the state λ in the parent nucleus and its analog in the daughter nucleus. In proton scattering experiments, the shift function $S_P(E_{rP})$ is the real part of the logarithmic derivative of an unbound state wave function. The excitation energies of low-lying resonances in parent nuclei are usually lower than the last neutron separation energy; in these cases $S_N(E_{rN})$ is the logarithmic derivative of a bound state wave function.[16]

The shift functions $S_P(E_{rP})$ and $S_N(E_{rN})$ were calculated with Coulomb wave functions and the bound neutron wave functions, respectively.[17] The reduced widths γ^2_λ were obtained from $\gamma^2_\lambda=\Gamma_{\lambda p}/2P$. The term $E_{\lambda P}-E_{\lambda N}$ contains the "normal" Coulomb energy shift, electromagnetic spin-orbit effects, etc. We assume that this term is constant and equal to 7.002 MeV, the excitation energy of the first analog resonance in ^{32}S.

The relative shifts of the analog and parent states in ^{32}P and ^{32}S are shown in Fig. 5. The fluctuations in the value of $E_x(^{32}\mathrm{S})-E_x(^{32}\mathrm{P})$ are directly related to the reduced widths of the states. If two states are close in energy, and one is much stronger than the other, the position of the stronger resonance can be moved so much that the order of the resonances in the daughter system is reversed with respect to the order in the parent system. For example, the analog of the $E_x(^{32}\mathrm{P})=4.010$ MeV, 2^- state is identified at $E_x(^{32}\mathrm{S})=10.977$ MeV ($\gamma^2=37.5$ keV, $\Delta_{PN}=-44.6$ keV), while the analog of the $E_x(^{32}\mathrm{P})=4.040$ MeV, 1^- state is identified at $E_x(^{32}\mathrm{S})=10.823$ MeV ($\gamma^2=153.4$ keV, $\Delta_{PN}=-173.6$ keV). This simple approximation accounts for about 70% of the observed relative shift between the parent and daughter states, providing additional evidence that the analog state assignments are correct.

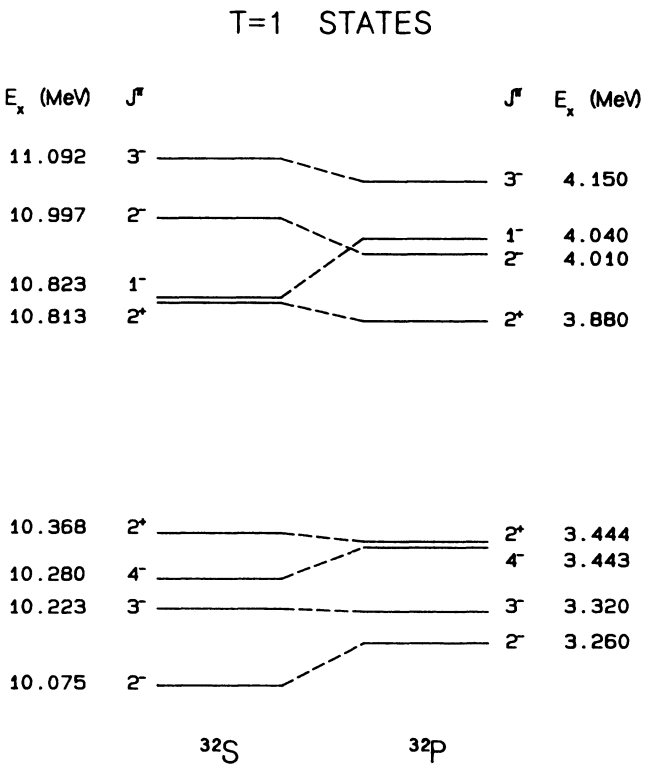

FIG. 5. Comparison of $T=1$ states in the parent nucleus ^{32}P and the daughter nucleus ^{32}S. For fragmented states, the centroid energy positions are plotted. Note that the order of the 1^- and 2^+ states is different in the two nuclei. The strong 1^- state has a very large Thomas-Ehrman shift.

C. Proton strength

Since the resonance laboratory width $\Gamma=2P\gamma^2$ contains the kinematic factor P, which usually varies several orders of magnitude for the energy range of our experiments, it is more reasonable to examine the reduced width γ^2. In Fig. 6 the reduced widths, cumulative reduced width, and positions of the resonances are plotted versus incident proton energy, for each l and J^π value. In Fig. 7 the same quantities are plotted for each s and J^π value. The reduced width $\gamma^2(E)$ plot gives the strength of the resonances and the strength distribution. The cumulative reduced width $\Sigma\gamma^2(E)$ shows the smoothness of the strength distribution. Any large fluctuation in strength is easily seen in this plot, which makes it useful in the identification of analog resonances.[12]

The top part of Fig. 6 shows the s-wave and d-wave strengths of ten 1^+ states. The cumulative reduced width strongly suggests that there is an analog resonance near $E_p=2.340$ MeV. A 1^+ state was found in the (d,p) reaction at $E_x(^{32}\mathrm{P})=4.200$ MeV. The energies also suggest that this resonance is an analog, but there is no reli-

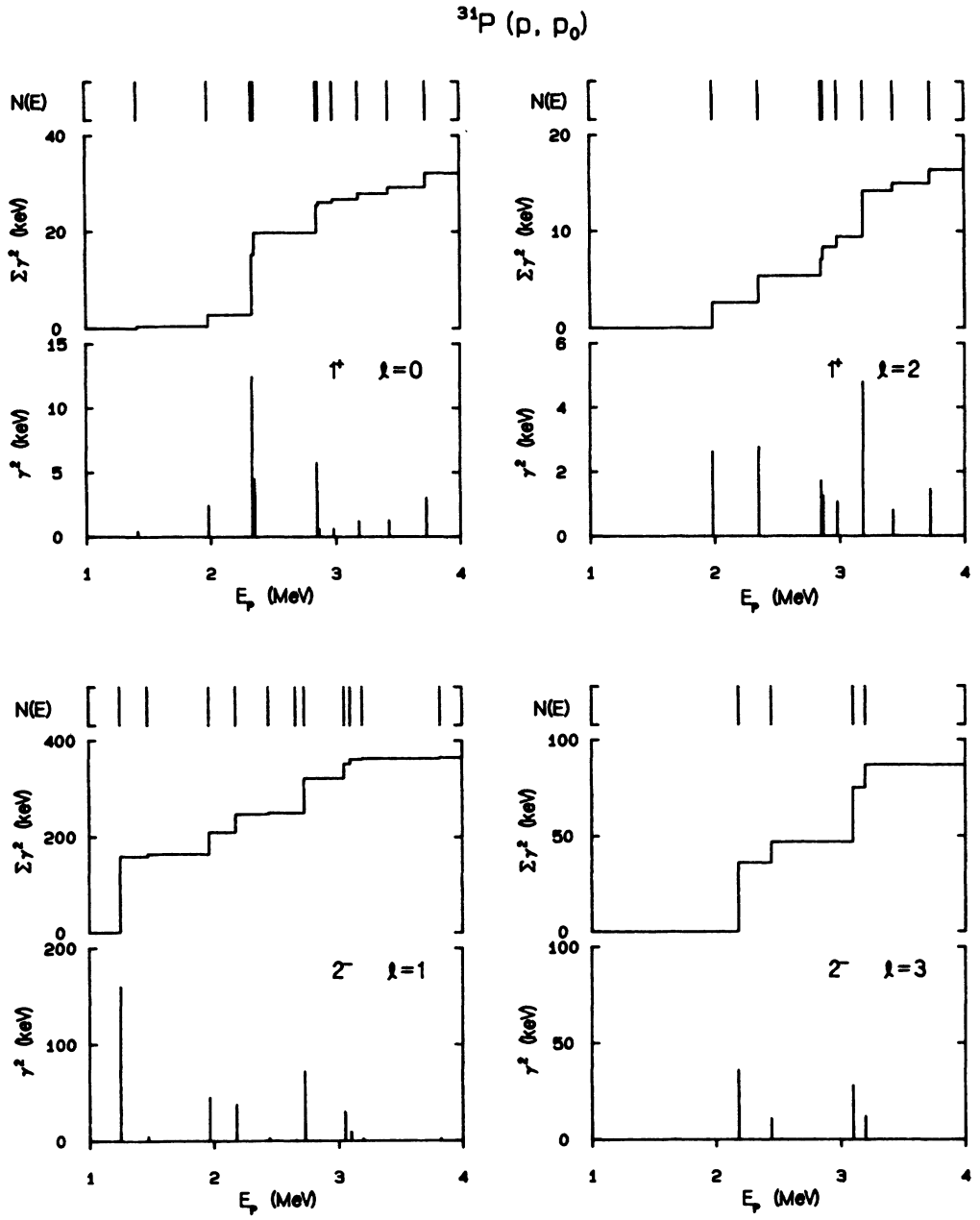

FIG. 6. Proton reduced widths vs energy for 1^+ and 2^- resonances in ^{32}S. The reduced widths are plotted for different l values.

able neutron strength information for comparison.

The 2^- resonances are shown in the bottom part of Fig. 6. The states are evenly distributed both in position and strength for $l=1$ and $l=3$. The l-mixing ratio is usually small. The resonance at $E_p=1.250$ MeV is a known analog resonance, and the resonance at $E_p=2.181$ MeV is identified as an analog in the present experiment.

Figure 7 (top part) shows the strength of thirty-three 1^- resonances for channel spin $s=0$ and $s=1$. Many of these states have α_0 decay. The shape of a 1^- resonance in elastic scattering, and the α_0 angular distribution for a 1^- state, are both very sensitive to the channel spin mixing ratio. Thus the strengths for different channel spins are better determined for 1^- resonances than for states with other J^π. The strengths are evenly distributed except for the analog resonance near 2.00 MeV.

The strength distribution for thirty-six 2^+ levels is shown in the middle part of Fig. 7 for the two channel spins. Since there is some ambiguity in determining the s-mixing ratio for 2^+ levels, the strengths for different s values are more uncertain than for 1^- states. The reso-

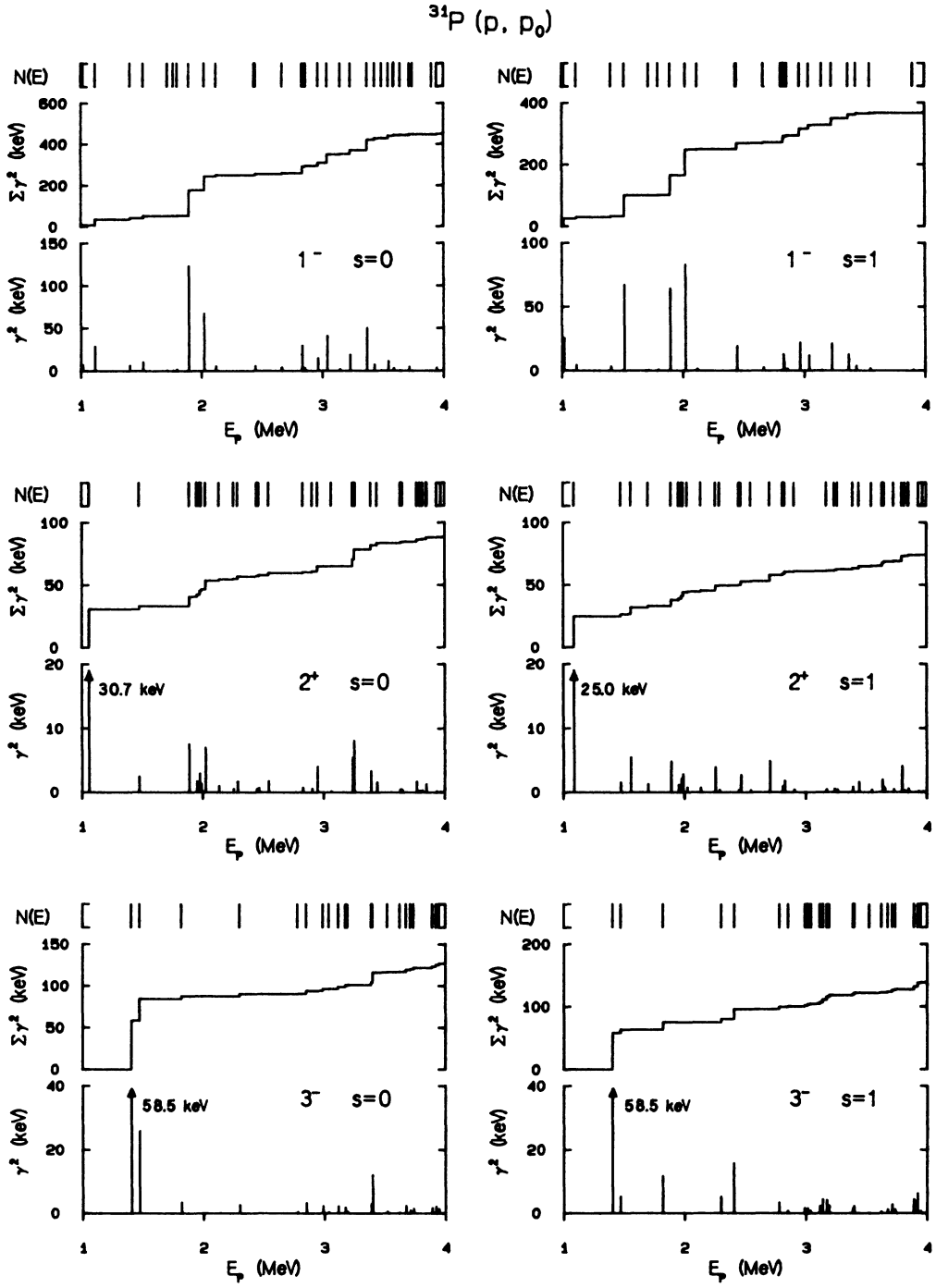

FIG. 7. Proton reduced widths vs energy for 1^-, 2^+, and 3^- resonances in ^{32}S. The reduced widths are plotted for different channels spins.

nances around $E_p = 2.00$ MeV are identified in the present experiment as fragments of an analog state. There also may be an analog state near $E_p = 3.23$ MeV, but there are no (d,p) data for comparison.

The strength information for twenty-five 3^- resonances is shown in the bottom part of Fig. 7. The strengths are again presented for the two channel spins. There are some uncertainties in the s-mixing ratios, especially for small resonances. The strong resonance at $E_p = 1.403$ MeV is an analog state.

D. Alpha strength

The energy region of the present experiment is above the $\alpha + ^{28}Si$ threshold at $E_x = 6.95$ MeV and below the $^{16}O + ^{16}O$ threshold at 16.54 MeV. The α decay widths

provide important information on the α-cluster structure. The alpha reduced widths for 1^-, 2^+, and 3^- resonances are shown in Fig. 8. It is convenient to consider the α strength in units of the Wigner limit: $\gamma_W^2 = 3\hbar^2/2ma^2$, where m is the reduced mass and a is the channel radius. In the present experiment, the average α strengths are small (about 0.02 γ_W^2), although several strong resonances are observed with widths about 0.10 γ_W^2. The strongest resonance with α_0 decay (at $E_p = 1.516$ MeV) has a reduced width of 0.27 γ_W^2.

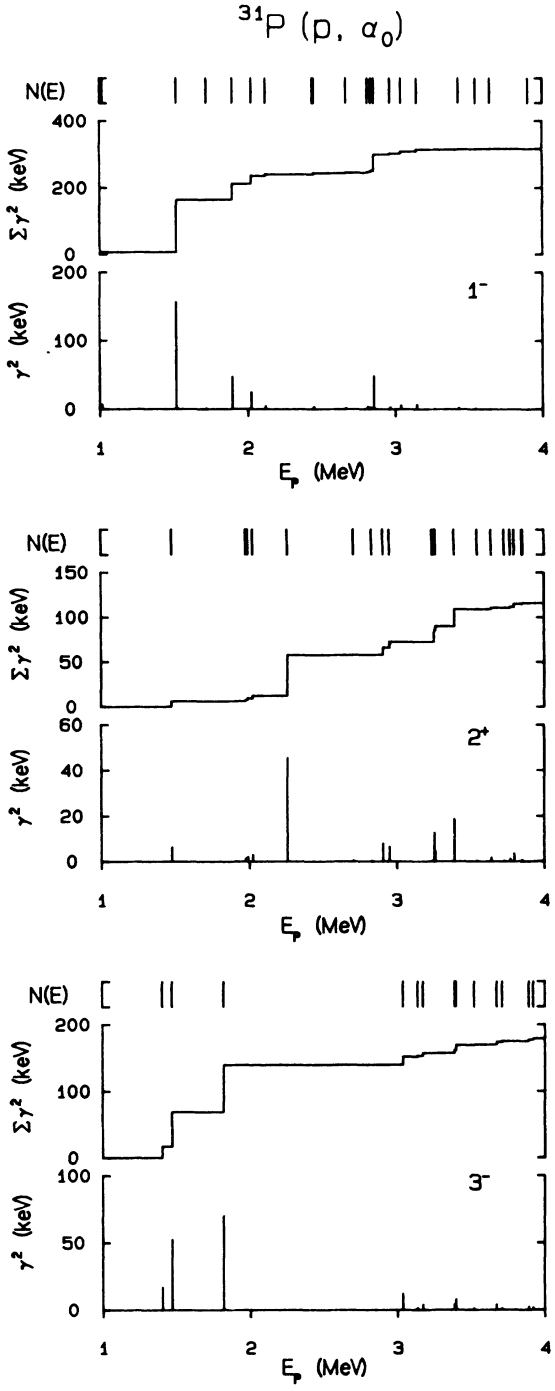

FIG. 8. Alpha reduced widths vs energy for 1^-, 2^+, and 3^- resonances in ^{32}S.

Since the α particle and the ground state of ^{28}Si have $T=0$, the analog resonances ($T=1$) should have zero α decay width if isospin is strictly conserved. However, the 2^+ analog states near $E_p = 2.00$ MeV have α decay. The resonance at $E_p = 2.022$ MeV has a reduced width $\gamma^2 = 0.04\ \gamma_W^2$. The energy and proton strength of this resonance agree well with the value obtained by Kalifa *et al.*[2] This state appears to have appreciable isospin mixing.

E. Comparison with shell model

Consider the states produced when a proton is added to a shell model orbit nlj. For a target nucleus with positive neutron excess $(N-Z)$, the isospin of the target is $T_t = (N-Z)/2$. The addition of a proton to the target leads to excited states with isospin $T = T_t \pm \frac{1}{2}$. The relations between the total spectroscopic strength for a proton added to the target and the number of the neutron and proton holes for the orbit nlj are[18]

$$G_p(T_<) = \frac{1}{N-Z+1}\langle \text{neutron holes}\rangle_{nlj} ,$$

$$G_p(T_>) = \langle \text{proton holes}\rangle_{nlj} - \frac{1}{N-Z+1}\langle \text{neutron holes}\rangle_{nlj} ,$$

where $\langle \text{holes}\rangle_{nlj}$ is the average number of holes in the orbit nlj.

In the present experiment $T_t = \frac{1}{2}$, $T_< = 0$, and $T_> = 1$. The spectroscopic strengths G_p are obtained from $G_p = \Gamma_p/\Gamma_{s.p.}$, where Γ_p is the observed laboratory width and $\Gamma_{s.p.}$ is the single particle width. The single particle widths were estimated by $\Gamma_{s.p.} = 2P(R)5\hbar^2/(8mR^2)$, where $P(R)$ is the penetrability of the Coulomb barrier at the radius $R = 1.25(A^{1/3}+1)$. Since this approximation reproduced the single particle widths for a number of resonances in this mass region,[12] it should be reliable enough for a qualitative comparison with the shell model predictions.

The resonance parameters obtained in the present experiment are in the LS coupling scheme, while the shell model calculations are in the jj representation. In the two schemes the same angular momenta—the spin of the incident particle i, the spin of the target I, and the orbital angular momentum l—are combined in two ways ($i+I=s$, $s+l=J$ and $i+l=j$, $I+j=J$). Without complete information (including signs) about the reduced width amplitudes, the transformation of the reduced widths from one representation to the other cannot be performed. However, if the signs of the amplitudes are assumed random, the reduced widths in the two representations have the relation

$$\gamma_j^2 = \sum_{sIJ} (2s+1)(2j+1)W^2(IiJl;sj)\gamma_{sIJ}^2 ,$$

where $W(IiJl;sj)$ is a Racah coefficient.

Transformed strengths and shell model calculations for the energy range of the present experiment are listed in Table III. The shell model predictions[2] were obtained by diagonalizing in the complete $d_{5/2}$-$s_{1/2}$-$d_{3/2}$ basis

TABLE III. Spectroscopic strengths.

nlj	Number of levels[a]	Present work $G_p(T_<+T_>)$[b]	Shell model calculation[c] $G_p(T_<)$	$G_p(T_>)$	$G_p(T_<+T_>)$
$1d_{5/2}$	45	0.106	0.032	0.100	0.132
$2s_{1/2}$	21	0.046	0.002	0.050	0.052
$1d_{3/2}$	48	0.109	0.001	0.084	0.085
$2p_{3/2}$	46	0.691			
$1f_{7/2}$	26	0.385			

[a]Note that due to s and l mixing, a single resonance often contributes to more than one nlj.
[b]G_p is the spectroscopic strength ($=\Gamma_p/\Gamma_{s.p.}$), $T_<=0$ and $T_>=1$.
[c]From Kalifa *et al.* (Ref. 2).

space a Hamiltonian which reproduces the single-hole spectrum of $A=39$ and simultaneously yields a root mean square best fit to a selected set of well-known level energies in the $A=32-38$ region. The spectroscopic factors for the ^{32}S resonances were calculated up to $E_x(^{32}\text{S})=14.60$ MeV. The present experiment provides data in the range $E_x=9.83-12.74$ MeV. Analog resonances are not identified for much of the energy range of this experiment, which makes the comparison for separate isospin questionable. We therefore compare only the total strengths (summed over the two T values); the experimental value agrees very well with the shell model calculations.

F. s-wave strength functions

The Bartlett spin-exchange force in the nucleon-nucleon interaction would result in a potential term which is dependent on the coupling of the spins of the incident nucleon (i) and the target nucleon (I). For s-wave resonances, this potential V' has the form[19]

$$V'=0.5[J(J+1)-I(I+1)-i(i+1)]V_2/A \ ,$$

where J is the spin of the compound nucleus, A is mass of the target and V_2 is a constant. This extra potential term vanishes for zero spin targets. For nonzero spin targets, two s-wave strength functions with different J values can be obtained. Previous measurements[5] for s-wave proton resonances in ^{28}Si obtained a ratio $S_{J=2}/S_{J=3}=3.5$, while the result[7] for s-wave resonances in ^{24}Mg was $S_{J=1}/S_{J=2}=0.61$. Proton resonance data on other odd-mass targets would be valuable to establish the systematics of the spin-spin dependence.

The large variation in s-wave strength function may be due to the small sample sizes. To determine the significance of a strength function ratio, Lynn[19] estimates the probability $P(0,b)$ that the observed ratio for two strength functions has a value equal to or larger than b, if the two samples are drawn from a Porter-Thomas distribution. [For $b<1$, the probability is $1-P(0,b)$.] In the present experiment $J_<=0$ and $J_>=1$. Measured s-wave strength functions $S_{J=0}$ and $S_{J=1}$ are 5.97×10^{-3} and 1.25×10^{-2}, respectively. The strength function ratio $S_{J=0}/S_{J=1}$ is 0.48 and the estimated probability for this ratio is only 0.05. This large difference in strength function is unlikely to reflect a true spin-spin effect, since there may be analog resonances among the 1^+ states. The (d,p) data provide energies and spins for states in the parent nucleus ^{32}P which correspond to $E_p>2.3$ MeV, but there is no reliable strength information. Thus the analogs can only be tentatively identified. If these possible analog resonances are eliminated, the s-wave strength functions are $S_{J=0}=5.97\times10^{-3}$ and $S_{J=1}=7.70\times10^{-3}$; the ratio $S_{J=0}/S_{J=1}=0.78$ has an estimated probability 0.29.

G. Applications to astrophysics

Understanding nucleosynthesis and energy generation during the oxygen burning phase of stellar evolution requires information on reaction rates for many nuclear reactions in the $A=32$ region. During explosive oxygen (and explosive silicon) burning, the reaction ^{28}Si(α,p)^{31}P plays an important role. The reaction ^{28}Si(α,p) is crucial for the final abundance of ^{31}P and ^{28}Si at the end of the oxygen burning stage and the abundance of ^{28}Si is clearly important for the future silicon burning stage. Here we use the present ^{31}P(p,α_0)^{28}Si resonance data and the principle of detailed balance to obtain ^{28}Si(α,p$_0$)^{31}P reaction rates. A more detailed description of this analysis will be published separately.[20]

The reaction rates at astrophysically interesting temperatures may be obtained by numerically integrating the equation[21]

$$\begin{aligned} N_A\langle\sigma v\rangle &= \int_0^\infty \sigma(v)v\phi(v,T)dv \\ &= 3.734\times10^{10}M^{1/2}T_9^{-3/2} \\ &\quad\times\int E\sigma(E)\exp(-11.605E/T_9) \\ &\quad\times dE \ \text{cm}^3\,\text{mol}^{-1}\,\text{s}^{-1} \ , \end{aligned}$$

where $\phi(v,T)$ is the Maxwellian distribution function, v is the relative velocity of the interacting particles, N_A is Avogadro's constant, $\sigma(E)$ is the measured reaction total cross section in barns, M is the reduced mass, and E is the center-of-mass energy in MeV.

Using the principle of detailed balance, the reaction rates for the reactions $1+2\rightarrow3+4+Q_{12,34}$, and $3+4\rightarrow1+2+Q_{34,12}$, where $Q_{12,34}$ and $Q_{34,12}$ are the reaction Q values, can be written as

$$\langle\sigma v\rangle_{34,12}=\langle\sigma v\rangle_{12,34}\left[\frac{M_{12}}{M_{34}}\right]^{3/2}\frac{(2J_1+1)(2J_2+1)}{(2J_3+1)(2J_4+1)} \times\exp\left[-\frac{Q_{12,34}}{kT}\right] ,$$

TABLE IV. Ground state thermonuclear reaction rates.

	$N_A\langle\sigma v\rangle_{p\alpha}$[a]		$N_A\langle\sigma v\rangle_{\alpha p}$[a]			Main
T_9	Present work	Theory[b]	Previous work[c]	Present work	Theory[b,c]	burning[d]
1.0	2.54×10^{1}		1.24×10^{-8}	3.92×10^{-9}	4.04×10^{-8}	HyC
1.5	1.59×10^{3}		3.11×10^{-4}	4.14×10^{-4}	1.01×10^{-3}	HyC
2.0	1.57×10^{4}		6.74×10^{-2}	1.75×10^{-1}	2.19×10^{-1}	ExC, HyOx
2.5	6.43×10^{4}		2.04×10^{0}	6.94×10^{0}	6.66×10^{0}	HyOx
3.0	1.64×10^{5}		2.25×10^{1}	8.11×10^{1}	7.33×10^{1}	ExOx
3.5	3.20×10^{5}	2.50×10^{5}	1.36×10^{2}	4.28×10^{2}	4.43×10^{2}	ExOx, ExSi
4.0	5.26×10^{5}		5.58×10^{2}	1.74×10^{3}	1.81×10^{3}	ExOx, ExSi
4.5	7.66×10^{5}	4.88×10^{5}	1.76×10^{3}	4.73×10^{3}	5.67×10^{3}	ExSi
5.0	1.03×10^{6}		4.58×10^{3}	1.08×10^{4}	1.46×10^{4}	ExSi
5.5	1.31×10^{6}		1.03×10^{4}	2.09×10^{4}		

[a] $N_A\langle\sigma\rangle_{p\alpha}$ and $N_A\langle\sigma v\rangle_{\alpha p}$ are the thermonuclear reaction rates for ^{31}P(p,α_0)^{28}Si and ^{28}Si(α,p$_0$)^{31}P. Reaction rates are in units of cm^3 mol^{-1} s^{-1}, while T_9 is in units of 10^9 K.

[b] Woosley *et al.* (Ref. 21).

[c] Buckby and King (Ref. 23).

[d] Hy is an abbreviation for hydrostatic and Ex for explosive; the notation is that of Clayton and Woosley (Ref. 22). For example, HyC is hydrostatic carbon burning and ExOx is explosive oxygen burning.

where M is the reduced mass of the channel. The function $\sigma(v)v\phi(v,T)$ has a maximum at $E=E_0$ for a certain temperature T_9, and there exists a "most effective" energy range $(E_0-\Delta E/2,\ E_0+\Delta E/2)$ in which interacting particle pairs make the main contribution to the thermonuclear reaction rates at that temperature.[22] If the temperature T_9 is in the range 1.0–10.0, then the "most effective energy" range for the ^{28}Si(α,p)^{31}P reaction is $E_\alpha^{\text{c.m.}}=1.26$–$10.95$ MeV. The thermonuclear reaction rates can be obtained either by measuring the (α,p$_0$) reaction directly or by measuring the inverse reaction (p,α_0) in the energy range $E_p^{\text{c.m.}}=0.0$–9.0 MeV. In the (α,p) measurement at low energies, the reaction yields are very small due to the large Coulomb barrier. The inverse reaction is easier to study. The integrated total cross section was obtained for ^{31}P(p,α_0)^{28}Si in the range $E_p^{\text{c.m.}}=0.97$–3.88 MeV. For ground state reactions, use of the (p,α) cross section and integrating the product of $\sigma(v)v\phi(v,T)$ gives the reaction rates at a particular temperature. The values for $N_A\langle\sigma v\rangle_{p\alpha}$ and $N_A\langle\sigma v\rangle_{\alpha p}$ are listed in Table IV.

The present results agree with the calculations by Woosley *et al.*[21] except at the lower end and upper range of temperatures. This is probably due to the absence of resonance parameters outside of the range $E_p^{\text{c.m.}}=0.98$–3.88 MeV. The reaction at lower temperatures may not be very important, since the ^{28}Si(α,p)^{31}P reaction is assumed to occur mostly at the stage of explosive carbon and explosive oxygen burning.

Buckby and King[23] measured the ^{28}Si(α,p)^{31}P reaction directly; their results are also listed in Table IV. Their reaction rates are lower than the present values by a factor of 2–3. However, the comparison is not direct, since their (α,p) measurement was only performed at 250 keV intervals with thin targets. Much of their energy region $(4.59\le E_\alpha^{\text{c.m.}}\le 10.5$ MeV) is beyond the effective energy range for $T_9=2.0$–5.0 $(2.0\le E_\alpha^{\text{c.m.}}\le 6.7$ MeV).

To determine ^{28}Si(α,p)^{31}P reaction rates at the explosive silicon burning $(3.5<T_9<5.5)$ stage, one needs either to measure the (α,p) reaction directly at higher energies, or to measure the (p,α) reaction at higher energies than in the present experiment.

V. SUMMARY

Differential cross sections for the ^{31}P(p,p$_0$), (p,p$_1$), (p,α_0), and (p,α_1) reactions were measured in the range $E_p=1.00$–4.01 MeV with an overall resolution about 400 eV. Resonance parameters were extracted for 143 levels with a multilevel, multichannel R-matrix code. Level-level interference effects were discussed. Eight isobaric analog resonances were identified in ^{32}S; one of them has a large Thomas-Ehrman shift. The spectroscopic factors are in excellent agreement with the (d,p) measurements for the parent states. The resonance strengths were compared with shell model predictions. There is good agreement when strengths for the two isospin values are summed. By using the principle of detailed balance, the thermonuclear reaction rates for the ^{28}Si(α,p$_0$)^{32}P reaction were evaluated from the ^{31}P(p,α_0)^{28}Si resonance parameters obtained in the present experiment. The reaction rates in the region $T_9=2$–5 are in good agreement with theoretical predictions.

ACKNOWLEDGMENTS

The authors would like to thank J. R. Vanhoy and J. F. Shriner, Jr. for helpful discussions, and B. J. Warthen, W. K. Brooks, J. S. Bull, L. H. James, K. J. Keeter, and B. W. Smith for assistance in performing the experiment. The work was supported in part by the U.S. Department of Energy under Contract Nos. DE-AC05-76ER01067 and DE-AS05-76ER03624.

[1]P. M. Endt and C. Van der Leun, Nucl. Phys. **A310**, 1 (1978).
[2]J. Kalifa, J. Vernotte, Y. Deschamps, F. Pougheon, G. Rotbard, M. Vergnes, and B. H. Wildenthal, Phys. Rev. C **17**, 1961 (1978).
[3]R. O. Nelson, E. G. Bilpuch, C. R. Westerfeldt, and G. E. Mitchell, Phys. Rev. C **27**, 930 (1983).
[4]R. O. Nelson, E. G. Bilpuch, C. R. Westerfeldt, and G. E. Mitchell, Phys. Rev. C **29**, 1656 (1984).
[5]R. O. Nelson, E. G. Bilpuch, C. R. Westerfeldt, and G. E. Mitchell, Phys. Rev. C **30**, 755 (1984).
[6]G. Adams, E. G. Bilpuch, C. R. Westerfeldt, and G. E. Mitchell, J. Phys. G **10**, 1747 (1984).
[7]J. R. Vanhoy, E. G. Bilpuch, C. R. Westerfeldt, and G. E. Mitchell, Phys. Rev. C **36**, 920 (1987).
[8]C. R. Westerfeldt, R. O. Nelson, E. G. Bilpuch, and G. E. Mitchell, submitted to Nucl. Instrum. Methods.
[9]C. R. Gould, L. G. Holzweig, S. E. King, Y. C. Lau, R. V. Poore, N. R. Roberson, and S. A. Wender, IEEE Trans. Nucl. Sci. **NS-28**, 3708 (1981).
[10]A. M. Lane and R. G. Thomas, Rev. Mod. Phys. **30**, 257 (1958).
[11]R. O. Nelson, E. G. Bilpuch, and G. E. Mitchell, Nucl. Instrum. Methods **A236**, 128 (1985).
[12]E. G. Bilpuch, A. M. Lane, G. E. Mitchell, and J. D. Moses, Phys. Rep. **28**, 145 (1976).
[13]S. A. A. Zaidi and S. Darmodjo, Phys. Rev. Lett. **19**, 1446 (1967).
[14]H. L. Harney, Nucl. Phys. **A119**, 591 (1968).
[15]W. M. Wilson, J. D. Moses, E. G. Bilpuch, and G. E. Mitchell, Nucl. Phys. **A227**, 277 (1974).
[16]H. A. Weidenmüller, Nucl. Phys. **69**, 113 (1965).
[17]L. I. Schiff, *Quantum Mechanics,* 3rd ed. (McGraw-Hill, New York, 1968).
[18]J. B. French and M. H. Macfarlane, Nucl. Phys. **26**, 168 (1962).
[19]J. E. Lynn, *The Theory of Neutron Resonance Reactions* (Clarendon, Oxford, 1968).
[20]D. F. Fang, F. J.Yang, E. G. Bilpuch, and G. E. Mitchell (unpublished).
[21]S. E. Woosley, W. D. Arnett, and D. D. Clayton, Astrophys. J. Suppl. Ser. **26**, 231 (1973).
[22]D. D. Clayton and S. E. Woosley, Rev. Mod. Phys. **46**, 755 (1974).
[23]M. A. Buckby and J. D. King, Can. J. Phys. **62**, 134 (1984).